sciendo

LATVIAN JOURNAL OF PHYSICS
AND TECHNICAL SCIENCES
2021, N 1

DOI: 10.2478/lpts-2021-0006

PEROVSKITE $CH_3NH_3PbI_{3-x}Cl_x$ SOLAR CELLS. EXPERIMENTAL STUDY OF INITIAL DEGRADATION KINETICS AND FILL FACTOR SPECTRAL DEPENDENCE

I. Kaulachs*[,1,2], A. Ivanova[2,3], A. Holsts[4], M. Roze[3], A. Flerov[5], A. Tokmakov[1], I. Mihailovs[1,3], M. Rutkis[1]

[1] Institute of Solid State Physics, University of Latvia,
8 Ķengaraga Str., Riga, LV-1063, LATVIA
[2] Institute of Physical Energetics,
11 Krīvu Str., Riga, LV-1006, LATVIA
[3] Institute of Applied Chemistry, Riga Technical University,
3 Paula Valdena Str., Riga, LV-1048, LATVIA
[4] Ltd Energolukss,
46/2 Ulbrokas Str, Riga, LV-1021, LATVIA
[5] Institute of Physics, University of Latvia,
32 Miera Str., Salaspils, LV-2169, LATVIA
* e-mail: igors.kaulacs@cfi.lu.lv

The main drawback of the methylammonium lead halide perovskite solar cells is their degradation in ambient atmosphere. To investigate ambient-air-induced cell degradation, spectral dependencies of open-circuit voltage (V_{OC}), fill factor (FF) and the power conversion efficiency (PCE) have been acquired (for the first time reported in literature).

Our custom-made measurement system allowed us to perform measurements of the above-mentioned entities *in situ* directly in vacuum during and after thermal deposition of the electrode. We also studied how these parameters in vacuum changed after cell exposure to ambient air for 85 min (50 nm top electrode) and for 180 min (100 nm top Ag electrode). For fresh $CH_3NH_3PbI_{3-x}Cl_x$ cell (never been in open air) with very high shunt resistance of $3 \cdot 10^7$ Ω·cm^2 (with practically no shorts and therefore FF could be determined mainly by charge carrier recombination processes) we found that FF in vacuum increased along with an increase of the incident photon energy from 0.55 at 760 nm up to 0.82 at 400 nm. Hypothesis considering hot

polaron participation in charge carrier photogeneration and recombination processes as well as another competing hypothesis were offered as possible explanations for the observed FF increase.

The kinetics of short-circuit photocurrent EQE with a change in pressure was also investigated. It was also shown that perovskite solar cell degradation could be noticeably reduced by increasing the top Ag electrode thickness to at least 100 nm, which could possibly facilitate the usual encapsulation process.

Keywords: *Degradation kinetics, fill factor spectral dependence, lead halide perovskite, power conversion efficiency, solar cells.*

1. INTRODUCTION

In the previous short literature review, we described the advantages of a low-temperature-developed inverted perovskite solar cell ITO/PEDOT:PSS/$CH_3NH_3PbI_{3-x}Cl_x$/$PC_{60}BM$/C_{60}/Ag and mentioned that the main drawback of it was degradation in ambient atmosphere [1]. Despite numerous reports existing about perovskite solar cell degradation during long periods of time such as days or months in ambient atmosphere, we did not find any report considering the degradation within short periods of time immediately after the deposition of the top electrode and the following vacuum change in the measurement chamber. Therefore, we developed a cell production and measuring system which allowed us to investigate kinetics of the first stage of degradation *in situ*, not only immediately after the top electrode deposition but also during the following decrease in vacuum up to the ambient atmospheric pressure and pumping back to the high vacuum (~$5 \cdot 10^{-7}$ torr). Thus, we present here the change kinetics of the short-circuit photocurrent (SCP) external quantum efficiency (EQE) during the slow decrease of the vacuum up to the ambient atmosphere conditions – as far as we know, for the first time in literature for such cells.

We found that an increase in the thickness of the top Ag electrode from 50 nm to 100 nm noticeably decreased the speed of cell degradation in the open air.

Spectral dependencies of other photovoltaic parameters such as open-circuit voltage (V_{OC}), power conversion efficiency (PCE) and fill factor (FF) were also acquired in the spectral range of 380–780 nm. Those measurements of spectral dependences are necessary for calculating spectral dependence of PCE, which may be a valuable parameter for solar cells if we need to use them for illumination that differ from full solar spectrum or if we want to enforce their parameters in some desirable spectral region by creating tandem sells. Those dependences can be used for "hunting" hot charge carrier presence in the cell. It is known than hot carriers in organic-inorganic perovskites give very long lifetime up to 100 ps and so they can appear in solar cells if one manages to receive them on electrodes. For the fresh cells with high shunt resistances of ~$2 \cdot 10^7$ Ω·cm^2, we observed a FF increase from 0.55 at 760 nm up to 0.82 at 400 nm, also for the first time reported in literature. Hypotheses to explain this phenomenon are offered in the present study.

2. EXPERIMENTAL

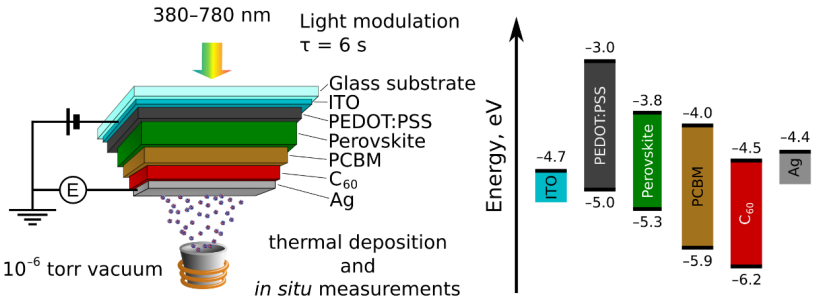

Fig. 1. The scheme of the experiment and the structure of the studied cells. The layers are sequentially deposited onto the bottom side, while the light is being shined from the top side.

The inverted planar mixed halide perovskite solar cells were fabricated with the following layer configuration: glass/ ITO/PEDOT:PSS/$CH_3NH_3PbI_{3-x}Cl_x$/ $PC_{61}BM/C_{60}$/Ag, using spin-coating from the solutions in the ambient atmosphere and, for the C_{60} and Ag electrode, by thermal vacuum evaporation – as reported previously [2]. The device structure, the energy level diagram of layers and the scheme of the experimental arrangement for *in situ* measurements are shown in Fig. 1.

2.1. Device Preparation: The Wet Part

Patterned ITO substrates (*PGO* 15 ohm/sq) were sequentially cleaned with chloroform, acetone, deionized (DI) water and isopropanol for 15 min each in an ultrasonic bath. After every sonication, the substrates were dump-rinsed in DI water. Poly(3,4-ethylenedioxythiophene) poly(styrenesulfonate) (PEDOT:PSS, *Clevios Baytron AI4083*) was deposited by spin-coating at 6500 rpm, at acceleration of 3000 rpm/s for 60 sec and annealed at 145 °C for 1 hour in the argon atmosphere. Then the perovskite absorber $CH_3NH_3PbI_{3-x}Cl_x$ was deposited by a modified interdiffusion method [3]: the mixture of PbI_2 (*Sigma Aldrich*, 99.999 % purity with trace metal bases) and $PbCl_2$ (*Sigma Aldrich*, 99.999 % purity with trace metal bases) with a molar ratio 3.4:1 was dissolved in the mixture of *N,N*-dimethylformamide (DMF; *Sigma Aldrich*, 99.8 %) and dimethylsulfoxide (DMSO; *Sigma Aldrich*, 99.9 %) with a molar ratio 3:1 [4], then spin-coated in the ambient air at a rate of 6500 rpm and acceleration of 3000 rpm/s at 65 °C for 75 s, using ~70 µL of 65 °C hot solution. The PbI_2:$PbCl_2$ film was dried as-fabricated for 20 minutes at the room temperature (rt) and for 20 minutes at 70 °C with an aim to remove the remaining solvents and to promote crystallization of the film. Then the cell was placed back on the hot spin-coater at 65 °C, after which ~90 µL of the hot 40 mg/mL methylammonium iodide (MAI; *Sigma Aldrich*, 99.9 %) solution in 2-propanol (IPA; *Sigma Aldrich*, 99.9 %) was squirted onto the middle of the cell, and after ~10 seconds the coating process was started at a speed of 6000 rpm with an acceleration of 3000 rpm/s and continued for 75 s.

Subsequently, the sample was put into

the thermostat at 50 °C, after which the temperature was slowly lifted up to 105 °C at a speed of 1.5 degree per minute. Annealing was continued for 1 h in the ambient air and then for 1 h in the argon atmosphere to finish the interdiffusion process; then the temperature was slowly decreased to the rt. Then the cell was covered with the $PC_{61}BM$ (*American Dye Source*, 99.5 %) layer from a 30 mg/mL solution in 1,2-dichlorobenzene (DCB; *Sigma Aldrich*, 99 %) by spin-coating at the speed of 2000 rpm and acceleration of 800 rpm/s, at the room temperature for 60 sec, using 50 μL of the solution. To improve the interdiffusion efficiency of the $PC_{61}BM$ into the perovskite along the grain boundaries and to remove the remaining solvents, the cell was again annealed for 1 hour in the argon atmosphere at 100 °C, slowly rising the temperature from 50 °C to 100 °C and then slowly lowering back to 50 °C.

2.2. Device Preparation: The Vacuum Part

Then an absorption spectrum of the cell was obtained, after which it was transferred to the custom-made vacuum system where about a 40 nm–thick C_{60} layer and an Ag electrode were thermally deposited in the vacuum of 10^{-6} torr. The photoelectric measurements were then performed *in situ*, without any moving of the cell. The double fullerene layer was used to passivate the deep and the shallow trap states [5]–[7]. The active cell area was 7 mm^2 according to the top electrode area. During the deposition of the top Ag electrode, the ohmic resistance and thickness of the electrode as well as the short-circuit current EQE were simultaneously measured while illuminating the cell via the bottom PEDOT:PSS electrode through the quartz window of the vacuum chamber by monochromatic light of 720 nm with an intensity of 10^{15} phot/(cm^2·s). Such a low quanta energy was used to avoid any possible photochemical processes in the cell.

Thus, the minimal thickness of the Ag electrode was chosen to be 50 nm, at which the value of the short-circuit photocurrent EQE reached its saturation while increasing the electrode thickness (as it will be shown further in the article, this thickness was enough to perform all the photoelectric measurements in vacuum but too low to protect the cell against fast degradation in the ambient air). The deposition speed and thickness of the thermally evaporated layers were checked by a calibrated 10 MHz quartz oscillator, frequency meter and computer-controlled shutter. The deposition speed for C_{60} was 6.5 Å/s at cell (sample) t = 25 °C. Before the deposition of the Ag electrode, the cell was cooled down a little to t = 13 °C to avoid a possible short-circuit, and the deposition speed was changed from 2 Å/s in the beginning up to 4.5 Å/s at the end of deposition for the 50 nm (thin) layer and to 7 Å/s for the 100 nm (thick) Ag.

2.3. In Situ Measurements

The cells were illuminated via the ITO electrode (see Fig. 1) by a chopper-modulated monochromatic light in the 370÷900 nm spectral region with an intensity of $10^9 \div 10^{15}$ phot/(cm^2·s), coming from a 250 W high-pressure xenon lamp through a grating monochromator. Appropriate filters were used to eliminate the second-order effects and the stray light. The selected light modulation period was chosen to be 6 s long, and the intensity was controlled by a calibrated Si photodiode. A constant photon flux onto our cell during the measurement of the spectral and the current–voltage

dependencies was achieved by computer-controlled movements of a *Thorlabs* linear variable ND metallic optical filter with the correction against the Si photodiode spectral sensitivity [8].

Synchrodetection technique [9] with the use of PC-controlled data storage, evaluating the mean value and the root-mean-square deviation (RMSD) allowed achieving the measurement accuracy of 1.5 %. The current (EQE)–voltage dependence measurements were made with a step of 0.05 V, the time for a single step varying from multiple minutes to 2 hours (depending on the level of the current noise) to ensure the aforementioned accuracy level of 1.5 % at the high-voltage end. After setting the next voltage value, a 20-second dead time was introduced to avoid the influence of transition processes. Hence, our EQE–voltage curves can be considered as if static. The magnitude of the dark current was permanently monitored by taking the endpoint value of the residual current during each dark half-period of the light modulation.

During the time-and-pressure-dependent SCP EQE evolution experiment, measurements were checked every 30–1000 light–dark periods, the light being adjusted to 10^{15} phot/(cm^2·s) with a relative error (the normalized root-mean-square deviation, NRMSD, calculated as the ratio of the RMSD to the mean value over the aforementioned 30–1000 periods) ± 1 %; for each period the mean value and the NRMSD of the EQE, the light intensity and the value of the photocurrent were collected. This made it possible to achieve the values of the NRMSD of the EQE from ~0.1 % to 0.4 %, and the measurement time of 2 to 55 minutes for each data point stored.

The ambient air that was let in during the experiment had the following properties: 760 torr pressure, ~40% relative humidity and ~22 °C temperature.

As noted before, the formation of perovskite degradation features of multiple volatile products [10]–[13] should be intensified under vacuum conditions. However, we checked this idea for a cell with 50 nm thin top electrode for two weeks in vacuum and observed a modest (~5 %) decrease in the short-circuit photocurrent EQE at 480 nm, whereas for the 620–720 nm region even a small increase in EQE was observed. Similarly, only minor changes in the properties were observed for the 100 nm thick top electrode cell after 2 months in vacuum.

3. RESULTS AND DISCUSSION

3.1. Cell with 50 nm (Thin) Ag Electrode

Figure 2 shows the dynamics of vacuum influence on the short-circuit photocurrent EQE for the inverted planar mixed-halide perovskite solar cell $CH_3NH_3PbI_{3-x}Cl_x$ by changing pressure in the measurement chamber from $3 \cdot 10^{-7}$ torr to the ambient air conditions (760 torr, ~40 % relative humidity, ~22 °C) and back to 10^{-6} torr for a 26-hour measurement period.

After shutting both the high- and low-vacuum valves, the vacuum slowly dropped from 3·10–7 torr to ~10–4 torr over 45 minutes. During this period, the value of the EQE did not change noticeably; however, 45 minutes later the EQE began to increase from 38.3 % to 43.2 %, which continued for 20 minutes (at this moment, 65 minutes had passed since the vacuum pumping was switched off). This peak value (~12 % higher than in high vacuum) remained for

~20 minutes (peak P in Fig. 2); then the EQE began to diminish, reaching its initial high-vacuum value after 2 hours, at which point the pressure in the measurement chamber dropped to 10^{-3} torr. A similar initial increase in the EQE for a direct mesoporous MAPbI3 perovskite solar cell was observed by Z. Song et al. [11]; this initial increase of the short-circui current EQE for the first 10÷20 minutes was explained by passivation of the surface trap states by the water molecules [14] and the improving contacts between the perovskite crystallites [15]. Song et al., however, carried out their measurements at a relative humidity (RH) of 55 % and 80 % at 1 atmosphere of the N_2 gas; we observed a similar effect.

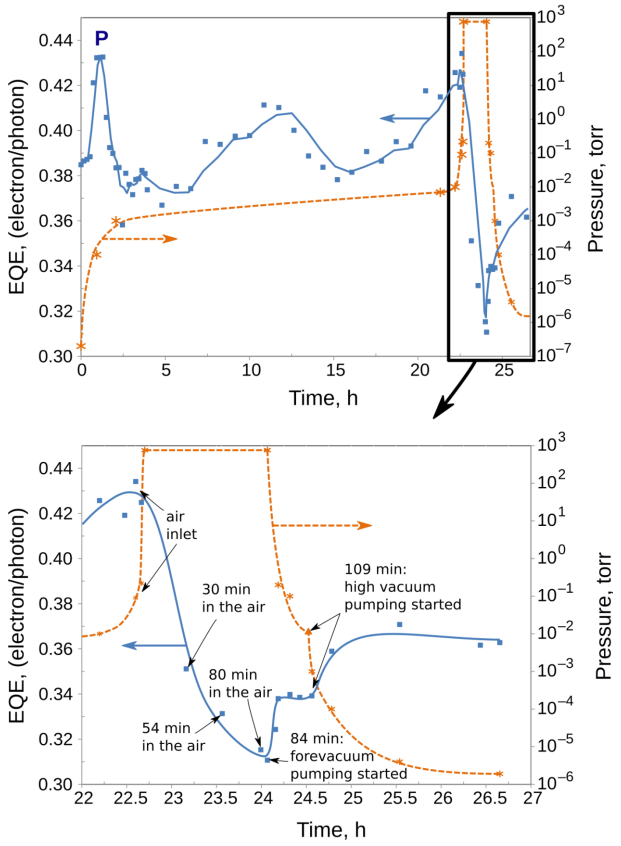

Fig. 2. Time dependence of the pressure change influence on the short-circuit EQE for the ITO/PEDOT:PSS/$CH_3NH_3PbI_{3-x}Cl_x$/$PC_{61}BM$/C_{60}/Ag cell with a 50 nm thick Ag electrode for 720 nm illumination with an intensity of 10^{15} phot/(cm^2·s). The curve within the top pane is based on moving average with a period of 5.

By decreasing vacuum from $3\cdot10^{-7}$ torr to ~10^{-4}–10^{-3} torr, the water vapour content in the chamber was lower by many orders of magnitude. Yet in our cell the Ag electrode was very thin (50 nm) and possibly very porous and, hence, easily penetrable by both H_2O and O_2; whereas Song et al. [11] used a dense and continuous gold electrode, relatively impenetrable to water. The water in our case could have originated in the gas phase by continuous desorption from the inner surface of the metallic walls of the measurement chamber and possibly by small leaks in the vacuum chamber (even a small concentration of water could lead to significant changes in the cell [14], [15]).

Here we must mention that by increasing the Ag electrode thickness to 100 nm, as well as its density, by faster evaporation (up to 7.5 Å/sec), this phenomenon was not so expressed anymore.

Then the system was left at slowly changing pressure for the time monitoring of the SCP EQE over ca. 20 h; the pressure slowly increased from 10^{-3} torr to 10^{-2} torr due to non-absolute hermeticity of the chamber. During this time, SCP EQE oscillated with a period of ~10 hours (see Fig. 2), characterizing the complicated diffusion processes of H_2O and O_2 into the cell through different layers and simultaneous back-diffusion of the perovskite destruction products out of the cell. After ~22-hour observation of the cell SCP EQE changes in the forevacuum, the ambient atmosphere (760 torr, 22 °C, RH ~ 40 %) was let into the measurement chamber, initially slowly by slightly opening the valve until the pressure reached $2 \cdot 10^{-1}$ torr (SCP EQE oscillations continued) and then by promptly opening the valve, at which point we observed a fast plunge of the photocurrent EQE from 43 % to 31 % during 85 minutes in the air (Fig. 2). However, as the vacuum pumping was restarted again, the SCP EQE increased back: first, during the period of ~15 minutes in the forevacuum of 10^{-1} torr, to 34 % and saturated at this value; second, when the high-vacuum pumping was started, to ~36–38 %. In addition, the spectral dependence of the SCP EQE remained practically unchanged after pumping back to $5 \cdot 10^{-7}$ torr (see Fig. 3; this pressure was achieved next day after the measurement depicted in Fig. 2 ended).

Here we see that the obtained EQE values are too moderate as it was also previously observed for the cells created by the interdiffusion method on the PEDOT:PSS HTL [16], possibly due to incomplete conversion of the PbI_2:$PbCl_2$ layer to perovskite after the deposition of the MAI layer and the following annealing of the cell. Such a situation is indeed sometimes observed when using a two-step interdiffusion method [16]–[18] where the excessive PbI_2 acts as an insulating layer, reducing the photocurrent [19]. This explanation is also supported by the very high values for shunt resistance (~$3 \cdot 10^7$ Ω·cm^2) and series resistance (R_{ser}; ~ 50÷60 Ω·cm^2) obtained for our cells (see Table 2).

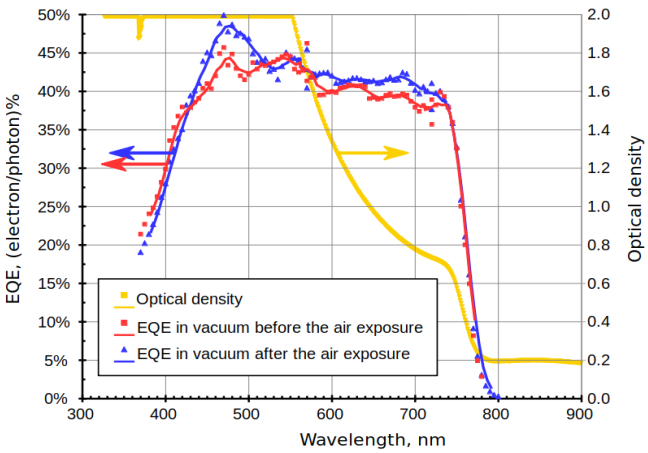

Fig. 3. Spectral dependences of the short-circuit photocurrent (SCP) EQE and the optical density of the perovskite and the PCBM layers for the cell with a 50 nm thick Ag electrode, before and after the exposure to air for 85 min. The curves are smoothed by moving average with a period of 5.

Table 1. The Change in the Electric Properties of the ITO/PEDOT:PSS/CH3NH3PbI3-xClx/PC61BM/C60 / Ag Cell with a 50 nm Thick Ag Electrode after the Air Inlet for 85 Minutes and Subsequent Pumping Back to Vacuum. The values given are the mean values with respect to the different directions of the applied voltage.

λ, nm	EQE, %		FF		V_{OC}, V		PCE, %	
	before	after	before	after	before	after	before	after
480	42	49	0.73	0.29	0.87	1.19	9.8	6.6
720	38	41	0.55	0.26	0.83	1.09	9.7	6.7

Table 2. The Change in the Electric Properties of the Cell With a 50 nm Thick Ag Electrode after the Air Inlet for 85 Minutes and Subsequent Pumping Back to Vacuum (average with respect to different directions of applied voltage).

λ, nm	R_{shunt}, Ω·cm²		R_{series}, Ω·cm²	
	before	after	before	after
480	$2.7 \cdot 10^7$	$2.3 \cdot 10^7$	47	640
720	$3.6 \cdot 10^7$	$2.4 \cdot 10^7$	52	670

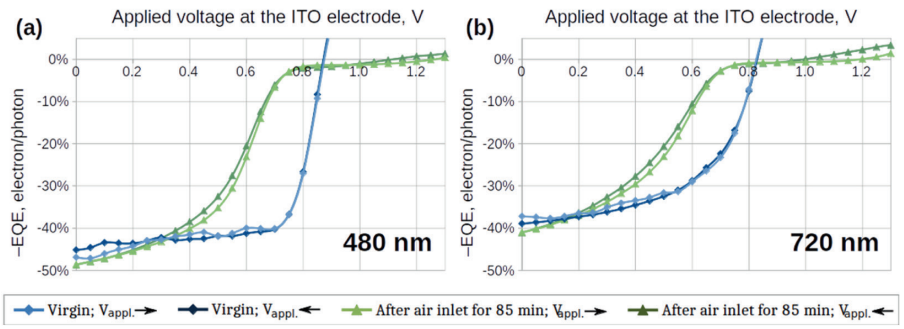

Fig. 4. The photocurrent EQE dependences on the externally ap¬plied voltage at '+' polarity of the ITO electrode for the light intensity of 10^{15} phot/(cm²·s) and (a) 480 nm or (b) 720 nm wavelength, measured in the vacuum of $5 \cdot 10^{-7}$ torr, for the sample with a 50 nm thick Ag electrode. The lighter curves stand for increasing voltage, the darker ones – for decreasing it; the EQE values are plotted with a negative sign, which indicates the electron flow direction towards the top Ag electrode.

Although the short-circuit photocurrent EQE in the vacuum did not change significantly after the exposure of the cell to the ambient air (as seen in Fig. 3), the EQE dependence on the applied voltage experienced dramatic changes after the air inlet for 85 minutes and subsequent pumping back to $5 \cdot 10^{-7}$ torr, when V_{OC} increased from 0.83 V to 1.1 V (for illumination with 720 nm) and from 0.87 V to 1.2 V (for illumination with 480 nm) – as shown both in Figs. 4 and 5 as well as in Table 1. At the same time, the fill factor (FF) decreased profoundly from 0.78 to 0.30 for 480 nm and from 0.55 to 0.26 for 720 nm, as seen in Table 1 and Fig. 6; see also Fig. 4.

After the cell exposure to the ambient air for 85 minutes, we observed that the shape of the current–voltage (CV) dependence on the cell noticeably changed (Fig. 4) and two distinct regions emerged. The dominant region (represented by dashed lines in Fig. 5) has now [extrapolated] V_{OC} values around ~0.60÷0.70 V, which are less than the values for the freshly made cell (0.83÷0.87 V). The FF corresponding to this dominant region is also lower after the cell exposure to the ambient air than it

was before the air inlet (see Fig. 6). One can conclude that, while the cell had stayed for 85 minutes in the ambient air, new charge-carrier recombination centers were irreversibly created in the cell, intensifying the recombination processes and thus leading to a decrease in both the fill factor and the V_{OC} for the dominant region.

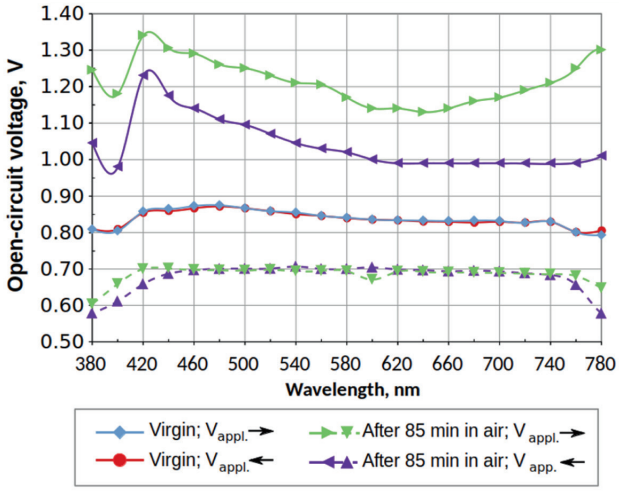

Fig. 5. Spectral dependences of the open-circuit voltage V_{OC}, measured in the vacuum of $5 \cdot 10^{-7}$ torr before and after the air inlet, for the sample with a 50 nm thick Ag electrode. The lighter curves stand for increasing voltage, the darker ones – for decreasing it; the dashed curves characterise the dominant region of the CV dependence plot.

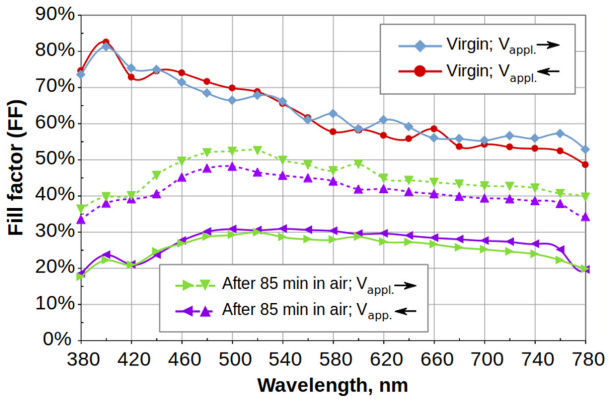

Fig. 6. Spectral dependences of the fill factor, measured in the vacuum of $5 \cdot 10^{-7}$ torr before and after the air inlet, for the sample with a 50 nm thick Ag electrode. The lighter curves stand for increasing voltage, the darker ones – for decreasing it; the finely dashed curves characterise the dominant region of the CV dependence plot.

Apart from the dominant region of the current–voltage characteristic, Fig. 4 also demonstrates a thin long tail over which the V_{OC} increases up to 1.2 V (at 480 nm) – and even higher for shorter wavelengths (Fig. 5). It indicates that after the air inlet into the measurement chamber not only charge recombination centers were cre-

ated but also some fraction of perovskite possibly degraded irreversibly to PbI_2. As it is known such degradation increases the bandgap up to 2.36 eV [10]. Barrier formation for the electron current at the contact of the perovskite layer with the Ag electrode after the air inlet cannot be ruled out, as the series resistance of the cell after the air inlet increased from 50÷60 $\Omega \cdot cm^2$ to more than 600 $\Omega \cdot cm^2$ (details in Table 2).

For this high-voltage tail of Fig. 4, a large hysteresis in the V_{OC} was observed with respect to the direction of the voltage change, as seen in Fig. 5. It indicates the appearance of a large number of the charge-carrier trapping centers after the air inlet. Possibly, these trapping centers intensify the recombination of the photogenerated charge carriers, consequently reducing the fill factor from 0.50÷0.82 for the cell that has only been in the vacuum to ~0.30 after the air was let in and then pumped back out to the high vacuum (as seen in Fig. 6).

For a virgin cell in the vacuum we found an interesting phenomenon: when increasing the energy of the light quanta of the excitation beam, the fill factor increased from 0.50 at 780 nm up to 0.82 at 400 nm, with a relatively steeper increase for the wavelengths shorter than ~600 nm (Fig. 6). The V_{OC} also experienced a mild increase along with an increase in the light quanta energy, as seen in Fig. 5. As far as we know, such a spectral dependence of the fill factor for a metal-organic perovskite solar cell has not been observed before.

At present, we cannot offer a convincing explanation of these phenomena but only propose some hypotheses discussing the hot polarons and their quasi-ballistic transport. It is known that at the room temperature after the photoexcitation, there are very long–lived hot charge carriers in the methyl ammonium lead halide perovskites. The lifetimes of such charge carriers are up to 100 ps [20]–[26], which is about two to three orders of magnitude longer than in the conventional semiconductors [25]. For the large charge-carrier densities (more than 10^{18} cm^{-3}), this is explained by the "hot phonon bottleneck", which originates from the reheating of the charge carriers due to the reabsorption of the phonons [20], [21], [24]. For much lower charge carrier densities of $\leq 10^{16}$ cm^{-3}, which occur under the solar flux and also in the experiments described in the present study, the long-living hot charge carriers can exist due to the formation of spatially large polarons determined by the fast motion of the methylammonium cation as well as the slower motions of the lead halide framework [22]. The reason for these outstandingly large lifetimes of the hot charge carriers is slow cooling of hot polarons by scattering on the acoustic phonons [25], and also by very low thermal conductivity of halide perovskites resulting from short phonon lifetimes [26].

The more the energy of exciting light quanta surpasses the bandgap, the hotter polarons are formed, with increasingly higher both the kinetic energy and the cooling time. Thus, for an excitation energy of 3.14 eV (1.49 eV above the bandgap) in $CH_3NH_3PbI_3$, a quasi-ballistic transport of the hot carriers is observed over up to 230 nm distance and a non-equilibrium transport over up to 600 nm in 100 ps after the excitation, as visualized by the ultrafast microscopy [25]. For lower excitation energy of 1.97 eV (0.32 eV above the band edge), on the other hand, only very little quasi-ballistic transport was detected [25]. Similarly, for the $CH_3NH_3PbI_{3-x}Cl_x$ perovskite (similar to the one in the present investigation) hot charge carriers with the lifetime above 100 ps were observed for the pump photon energies of 3.1 eV and 2.6 eV but were not observed for lower pump energies of 2.05 eV in 100 ps after the excitation [24].

During the quasi-ballistic transport, the charge carriers interact weakly with the trapping centers [24], [25]; therefore, few of them undergo recombination during the transport through the perovskite layer. This can explain the observed increase of the fill factor (which depends directly on the charge carrier recombination) when increasing the photon energy above ~ 2.07 eV (600 nm), as shown in Fig. 6: the higher energy the charge carrier possesses, the longer the distance it travels quasi-ballistically. If it were possible to collect most of these charge carriers at the electrodes, we would observe a strong increase in the V_{OC} value when increasing the incident photon energy above 2.07 eV – but only a small increase from 0.83 eV to 0.87 eV was detected (see Fig. 5), probably because there were substantial losses of the kinetic energy of the hot charge carriers both at the interfaces and inside the charge transport layers, possibly including the insulating layer of PbI_2:$PbCl_2$ (in front of the PEDOT:PSS layer), which remained unconverted from the interdiffusion process when the cell was created.

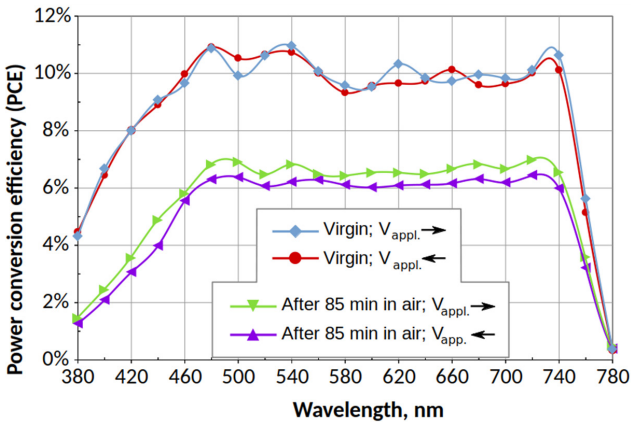

Fig. 7. Spectral dependences of the power conversion efficiency (PCE), measured in the vacuum of $5 \cdot 10^{-7}$ torr before and after the air inlet for 85 min, for the sample with a 50 nm thick Ag electrode. The lighter curves stand for increasing voltage, the darker ones – for decreasing it.

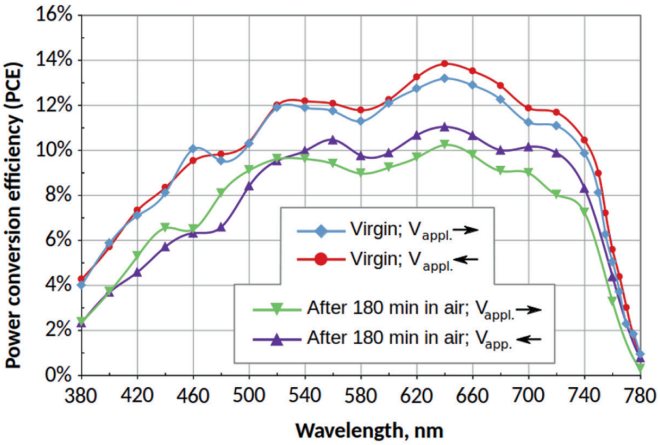

Fig. 8. Spectral dependences of the power conversion efficiency (PCE), measured in the vacuum of $5 \cdot 10^{-7}$ torr before and after the air inlet for 180 min, for the sample with a 100 nm thick Ag electrode. The lighter curves stand for increasing voltage, the darker ones – for decreasing it.

After the cell was exposed to the ambient air for 85 minutes, there was no increase in the FF when moving to the wavelengths of the excitation light shorter than 600 nm anymore (Fig. 6). This could be explained by accumulation of the perovskite degradation product PbI_2, which strongly increased the cooling rate of the hot carriers (observed for the cells produced using a two-step method [20]), and, possibly, by the contact degradation of the Ag electrode, marked by an increase in series resistance of the cell from ~ 50 Ω·cm^2 to more than 600 Ω·cm^2 (Table 2).

Nevertheless, the observed phenomena can also be explained by another hypothesis: when a cell accommodating a large number of the charge carrier traps absorbs light and if the photon energy exceeds the depth of a filled trap plus the applied (external) voltage multiplied by the electron charge, the charge carriers can now go in the opposite direction to the applied external voltage due to energetic considerations. This direction coincides with the flow direction of the charge carriers in the absence of the applied external field. The higher the energy of the photon, the more excess energy is received by the charge carrier released from a trap, and hence the easier it can overcome the applied external field. This, in turn, produces higher opposite-direction extra current, which changes the shape of the photocurrent EQE dependence on the applied voltage in the region of high voltages. Consequently, the observed fill factor should be larger, as is actually seen in Fig. 6 (compare also the curves for the virgin cell in Figs. 4a and 4b). Such a situation is possible when the local electric field in the cell is strongly non-uniform and when some processes of trap filling from external sources take place. Such a process can be the dark injection from the electrodes. Still, this is only a hypothesis, and at present we have no exact explanation for an increase in the FF when increasing the incident photon energy.

Using the obtained spectral dependences for the EQE, the FF and the V_{OC}, we can construct spectral dependences for the power conversion efficiency (PCE) using the following formula [8]:

$$PCE = \frac{V_{OC} \cdot FF \cdot EQE}{E_{phot}}, \quad (1)$$

where V_{OC} – the open-circuit voltage, V;
FF – the fill factor;
EQE – the external quantum efficiency for the short-circuit photocurrent;
E_{phot} – the incident photon energy, eV.

The PCE spectral dependences for the cell with a 50 nm thin electrode are shown in Fig. 7. This quantity is rather constant within the range of 480–740 nm, despite the fact that the optical density of the sample varies significantly between 550 and 740 nm. One reason is the Ag top electrode (not present when the absorption spectrum was acquired) acting as a mirror for the light to pass multiple times in the sample, thus facilitating more complete absorption. It can also be seen that after the exposure to the ambient air, the PCE decreased 1.5 times at 720 nm, and even more at wavelengths shorter than 460 nm. At 400 nm, this decrease in the PCE even approached 3 times. This is mainly due to a dramatic decrease in the fill factor, as seen in Table 1 and Fig. 6. Much lesser degradation of the cell performance under the exposure to the ambient air was observed for the cell with increased thickness of the top Ag electrode (100 nm instead of 50 nm). This will be discussed in the following section of the article.

3.2. Cell with 100 nm (Thick) Ag Electrode

The spectral dependences of the PCE for the cell with a 100 nm thick Ag electrode are shown in Fig. 8. This cell experienced a twice as long (180 min) exposure to the ambient atmosphere in the measurement chamber compared to the one with a thin electrode; nevertheless, as can be seen in Fig. 8, the PCE suffered much lesser reduction for this cell (compare Figs. 8 and 7). Here we must admit that both cells are not absolutely identical because the one with a thick electrode shows lower PCE values in the short-wavelength region, possibly indicating a thicker layer of the leftover PbI2:PbCl2 left unconverted during cell fabrication. In addition, the shunt resistance for the thick-electrode cell is about an order of magnitude lower than for the thin-electrode cell – this is probably evidence of higher pinhole concentration. Yet we hope that these differences do not obstruct the comparison of the Ag electrode protecting properties in both cases: the diminution of the PCE for the cell with a 100 nm thick electrode is only 1.2 times at 720 nm and 1.6 times at 400 nm (Fig. 8 and Table 3) while for the cell with a 50 nm thick electrode, exposed to the ambient air for half as long, it was 1.5 times at 720 nm and ~3 times at 400 nm. The series resistance for the cell with a thicker Ag electrode increased from 30÷35 Ω·cm^2 to 50÷60 Ω·cm^2 after a 180 min exposure (see Table 4) while for the cell with a thinner electrode the increase was much stronger, from ~50 Ω·cm^2 to 640÷670 Ω·cm^2, for only 85 min exposure (see Table 2). The decrease in the fill factor after the exposure to the ambient air was also much smaller for the cell with 100 nm thick top Ag electrode than for the cell with 50 nm thick Ag electrode (compare Table 3 with Table 1). We can conclude that the increase in the top Ag electrode thickness just by 50 nm (from 50 nm to 100 nm) significantly improves the protection of the cell from the ambient atmosphere influence. Therefore, it becomes possible to perform subsequent encapsulation under ambient conditions instead of the glovebox.

Table 3. The Change in the Electric Properties of the ITO/PEDOT:PSS/$CH_3NH_3PbI_{3-x}Cl_x$/$PC_{61}BM$/C_{60}/Ag Cell with a 100 nm Thick Ag Electrode after the Air Inlet for 180 Minutes and Subsequent Pumping Back to Vacuum. The values given are the mean values with respect to the different directions of the applied voltage.

λ, nm	EQE, %		FF		V_{oc}, V		PCE, %	
	before	after	before	after	before	after	before	after
480	45	36	0.64	0.52	0.88	0.92	9.7	6.4
720	39	39	0.60	0.51	0.83	0.85	11	9.6

Table 4. The Change in the Electric Properties of the Cell with a 100 nm Thick Ag Electrode after the Air Inlet for 180 Minutes and Subsequent Pumping Back to Vacuum (average with respect to different directions of applied voltage)

λ, nm	R_{shunt}, Ω·cm^2		R_{series}, Ω·cm^2	
	before	after	before	after
480	3.1·10^6	2.0·10^6	35	64
720	3.9·10^6	2.2·10^6	31	52

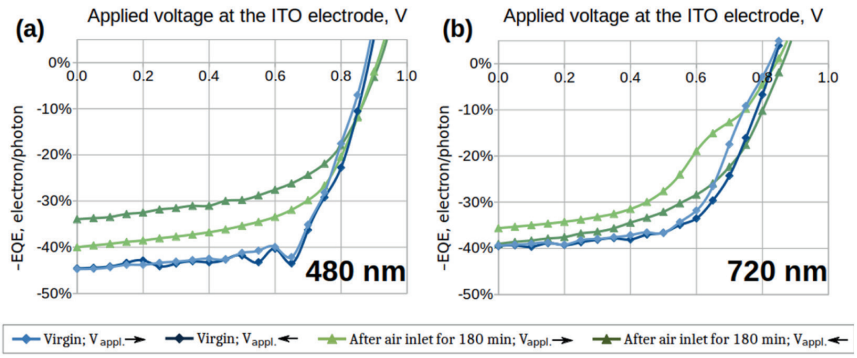

Fig. 9. The photocurrent EQE dependences on the externally applied voltage at '+' polarity of the ITO electrode for the light intensity of 10^{15} phot/(cm^2·s) and (a) 480 nm or (b) 720 nm wavelength, measured in the vacuum of $5 \cdot 10^{-7}$ torr, for the sample with a 100 nm thick Ag electrode. The lighter curves stand for increasing voltage, the darker ones – for decreasing it; the EQE values are plotted with a negative sign, which indicates the electron flow direction towards the top Ag electrode.

Finally, the current–voltage characteristics changed less after the exposure to the air for the 100 nm–thick-Ag-electrode cell. It should be noted that the two regions observed on these plots for the 50 nm–thick-Ag-electrode cell are not present for the 100 nm–thick-Ag-electrode cell anymore: no long-tail region as in Fig. 4 is visible in Fig. 9. Only some decrease in the EQE values and the appearance a noticeable hysteresis are present, which indicates that even the protection offered by the 100 nm thick Ag layer is not enough to ensure the cell stability over a period of 180 minutes in the ambient air.

4. CONCLUSIONS

For inverted planar mixed halide perovskite $CH_3NH_3PbI_{3-x}Cl_x$ solar cells, the fill factor was found to increase when increasing the energy of the excitation photons: from 0.55 at 760 nm up to 0.82 at 400 nm for a freshly prepared cell with a 50 nm thick top Ag electrode, which had very high shunt resistance R_{shunt} of $3 \cdot 10^7$ Ω·cm^2. Such high resistances indicate the low content of pinholes; in such a case the FF is mainly established by the recombination processes of the photogenerated charge carriers in the cell. This increase could be caused by hot polaron formation; the higher polaron energy, the lower their recombination. Also, other hypothetical explanations cannot be excluded. Thus, spectral dependences for the FF and the V_{OC} can provide an additional insight into the photovoltaic processes in the cell.

The kinetics of initial evolution of short-circuit photocurrent (SCP) EQE when vacuum was changed slowly from 5.10^{-7}torr to ambient atmosphere and pumped back to high vacuum was investigated. When initially vacuum diminished to ~ 10^{-4} torr even some increase of EQE was observed for cell with thin Ag electrode. This could be caused by incoming water molecules passivating surface trap states and/or improving intergrain contacts. By further decrease of vacuum some long period oscilations of SCP EQE were observed due to intricate diffusion processes of H_2O and O_2 until~$2 \cdot 10^{-1}$ torr was reached. Letting the ambient air into the measurement chamber

caused a steep fall in EQE, but after the vacuum pumping was restarted, nearly initial values of the SCP EQE were observed again. Hence, this change for SCP EQE spectral dependence is reversible. However, spectral dependences for FF and V_{OC} bore strong evidence of irreversible degradation where FF diminished to less than 0.3 in the whole investigated spectrum, but V_{OC} dependence tail part increased up to 1.3 V at 420 nm. Thus, we can conclude that to get more full information about degradation processes in the cell we ought to investigate also spectral dependences for FF and V_{OC}, not only for SCP EQE

It was observed that the speed and the paths of degradation after the air inlet into the measurement chamber were strongly dependent on the thickness of the top Ag electrode. It means that for a 50 nm thick top electrode, exposure of the cell to the ambient air for 85 minutes and subsequent pumping back to $5 \cdot 10^{-7}$ torr induced dramatic changes in the shape of the current–voltage characteristics and thus in the V_{OC} and the FF. On the other hand, for the cell with a 100 nm thick top electrode, exposure to the ambient air for twice as longer period of 180 minutes and following pumping back led only to a moderate fall in the FF, whereas the shape of the current–voltage characteristics changed considerably less. Therefore, top Ag electrode thickness of at least 100 nm is recommended to increase the lifetime of the cells before their encapsulation.

ACKNOWLEDGEMENTS

Institute of Solid State Physics, University of Latvia as the Centre of Excellence has received funding from the European Union's Horizon 2020 Framework Programme H2020-WIDESPREAD-01-2016-2017-Teaming Phase2 under grant agreement No. 739508, project CAMART².

REFERENCES

1. Kaulachs, I., Ivanova, A., Holsts, M., Roze, A., Flerov, A., Tokmakov, A., Mihailovs, I., & Rutkis, M. (2020). Perovskite $CH_3NH_3PbI_{3-x}Cl_x$ Solar Cells And Their Degradation (Part 1: A Short Review). *Latv. J. Phys. Tech. Sci. 2021, 1*, 44 -52. DOI: 10.2478/lpts-2021-0005.
2. Ivanova, A., Tokmakov, A., Lebedeva, K. Roze, M., & Kaulachs, I. (2017). Influence of the Preparation Method on Planar Perovskite $CH_3NH_3PbI_{3-x}Cl_x$ Solar Cell Performance and Hysteresis. *Latv. J. Phys. Tech. Sci.*, *54*, 58–68. DOI: 10.1515/lpts-2017-0027.
3. Xiao, Z., Bi, C., Shao, Y., Dong, Q., Wang, Q., Yuan, Y., … & Huang, J. (2014). Efficient, High Yield Perovskite Photovoltaic Devices Grown by Interdiffusion of Solution-Processed Precursor Stacking Layers. *Energy Environ. Sci., 7*, 2619–2623. DOI: 10.1039/C4EE01138D.
4. Seo, Y.-H., Kim, E.-C., Cho, S.-P., Kim, S.-S., & Na, S.-I. (2017). High-Performance Planar Perovskite Solar Cells: Influence of Solvent upon Performance. *Appl. Mater. Today*, *9*, 598–604. DOI: 10.1016/j.apmt.2017.11.003.
5. Shao, Y., Xiao, Z., Bi, C., Yuan, Y., & Huang, J. (2014). Origin and Elimination of Photocurrent Hysteresis by Fullerene Passivation in $CH_3NH_3PbI_3$ Planar Heterojunction Solar Cells. *Nat. Commun., 5*, 5784. DOI: 10.1038/ncomms6784.

6. Lopez-Varo, P., Jiménez-Tejada, J.A., García-Rosell, M., Ravishankar, S., Garcia-Belmonte, G., Bisquert, J., & Almora, O. (2018). Device Physics of Hybrid Perovskite Solar cells: Theory and Experiment. *Adv. Energy Mater*., *8*, 1702772. DOI: 10.1002/aenm.201702772.
7. Wang, Q., Shao, Y., Dong, Q., Xiao, Z., Yuan, Y., & Huang, J. (2014). Large Fill-Factor Bilayer Iodine Perovskite Solar Cells Fabricated by a Low-Temperature Solution-Process. *Energy Environ. Sci., 7*, 2359–2365. DOI: 10.1039/C4EE00233D.
8. Kaulachs, I., Muzikante, I., Gerca, L., Shlihta, G., Shipkovs, P., Grehovs, V., … & Ivanova, A. (2012). Electrodes for GaOHPc:PCBM/P3HT:PCBM Bulk Heterojunction Solar Cell. *Chem. Phys., 405*, 46–51. DOI: 10.1016/j.chemphys.2012.06.007.
9. Kaulachs, I., & Silinsh, E. (1994). Molecular Triplet Exciton Generation via Optical Charge Transfer States in A-Metalfree Phthalocyanine, Studied by Magnetic Field Effects. *Latv. J. Phys. Tech. Sci.*, *5*, 12–22.
10. Shahbazi, M., & Wang, H. (2016). Progress in Research on the Stability of Organometal Perovskite Solar Cells, *Sol. Energy.*, *123*, 74–87. DOI: 10.1016/j.solener.2015.11.008.
11. Song, Z., Abate, A., Watthage, S.C., Liyanage, G.K., Phillips, A.B., Steiner, U., … & Heben, M.J. (2016). Perovskite Solar Cell Stability in Humid Air: Partially Reversible Phase Transitions in the PbI_2-CH_3NH_3I-H_2O System. *Adv. Energy Mater.*, *6*, 1600846. DOI: 10.1002/aenm.201600846.
12. Wang, Q., Chen, B., Liu, Y., Deng, Y., Bai, Y., Dong, Q., & Huang, J. (2017). Scaling Behavior of Moisture-Induced Grain Degradation in Polycrystalline Hybrid Perovskite Thin Films. *Energy Environ. Sci*., *10*, 516–522. DOI: 10.1039/C6EE02941H.
13. Wang, D., Wright, M., Elumalai, N.K., & Uddin, A. (2016). Stability of Perovskite Solar Cells. *Sol. Energy Mater. Sol. Cells*, *147*, 255–275. DOI: 10.1016/j.solmat.2015.12.025.
14. Zhou, W., Zhao, Y., Shi, C., Huang, H., Wei, J., Fu, R., ... & Zhao, Q. (2016). Reversible Healing Effect of Water Molecules on Fully Crystallized Metal–Halide Perovskite Film. *J. Phys. Chem. C.*, *120*, 4759–4765. DOI: 10.1021/acs.jpcc.5b11465.
15. Eperon, G.E., Habisreutinger, S.N., Leijtens, T., Bruijnaers, B.J., van Franeker, J.J., DeQuilettes, D.W., … & Snaith, H.J. (2015). The Importance of Moisture in Hybrid Lead Halide Perovskite Thin Film Fabrication. *ACS Nano*., *9*, 9380–9393. DOI: 10.1021/acsnano.5b03626.
16. Zhao, D., Sexton, M., Park, H.-Y., Baure, G., Nino, J.C., & So, F. (2015). High-Efficiency Solution-Processed Planar Perovskite Solar Cells with a Polymer Hole Transport Layer. *Adv. Energy Mater.*, *5*, 1401855. DOI: 10.1002/aenm.201401855.
17. Shi, Z., & Jayatissa, A. (2018). Perovskites-Based Solar Cells: A Review of Recent Progress, Materials and Processing Methods. *Materials (Basel)*, *11*, 729. DOI: 10.3390/ma11050729.
18. Wang, Q., Shao, Y., Xie, H., Lyu, L., Liu, X., Gao, Y., & Huang, J. (2014). Qualifying Composition Dependent p and n Self-Doping in CH3NH3PbI3. *Appl. Phys. Lett.*, *105*, 163508. DOI: 10.1063/1.4899051.
19. Chen, Q., Zhou, H., Song, T.-B., Luo, S., Hong, Z., Duan, H.-S., … & Yang, Y. (2014). Controllable Self-Induced Passivation of Hybrid Lead Iodide Perovskites toward High Performance Solar Cells. *Nano Lett.*, *14*, 4158–4163. DOI: 10.1021/nl501838y.
20. Yang, Y., Ostrowski, D.P., France, R.M., Zhu, K., van de Lagemaat, J., Luther, J.M., & Beard, M.C. (2016). Observation of a Hot-Phonon Bottleneck in Lead-Iodide Perovskites. *Nat. Photonics*, *10*, 53–59. DOI: 10.1038/nphoton.2015.213.
21. Niesner, D., Zhu, H., Miyata, K., Joshi, P.P., Evans, T.J.S., Kudisch, B.J., … & Zhu, X.-Y. (2016). Persistent Energetic Electrons in Methylammonium Lead Iodide Perovskite Thin Films. *J. Am. Chem. Soc.*, *138*, 15717–15726. DOI: 10.1021/jacs.6b08880.

22. Yang, J., Wen, X., Xia, H., Sheng, R., Ma, Q., Kim, J., … & Conibeer, G. (2017). Acoustic-Optical Phonon Up-Conversion and Hot-Phonon Bottleneck in Lead-Halide Perovskites. *Nat. Commun.*, *8*, 14120. DOI: 10.1038/ncomms14120.
23. Zhu, H., Miyata, K., Fu, Y., Wang, J., Joshi, P.P., Niesner, D., ... & Zhu, X.-Y. (2016). Screening in Crystalline Liquids Protects Energetic Carriers in Hybrid Perovskites. *Science*, *353*, 1409–1413. DOI: 10.1126/science.aaf9570.
24. Bretschneider, S.A., Laquai, F., & Bonn, M. (2017). Trap-Free Hot Carrier Relaxation in Lead–Halide Perovskite Films. *J. Phys. Chem. C.*, *121*, 11201–11206. DOI: 10.1021/acs.jpcc.7b03992.
25. Guo, Z., Wan, Y., Yang, M., Snaider, J., Zhu, K., & Huang, L. (2017). Long-Range Hot-Carrier Transport in Hybrid Perovskites Visualized by Ultrafast Microscopy. *Science*, *356*, 59–62. DOI: 10.1126/science.aam7744.
26. Frost, J.M., Whalley, L.D., & Walsh, A. (2017). Slow Cooling of Hot Polarons in Halide Perovskite Solar Cells. *ACS Energy Lett*., *2*, 2647–2652. DOI: 10.1021/acsenergylett.7b00862.